Materials and Design 193 (2020) 108814

Contents lists available at ScienceDirect

Materials and Design

journal homepage: www.elsevier.com/locate/matdes

Mechanical response and microstructure evolution of commercially pure titanium subjected to repetitive bending under tension

Saeed Tamimi [a,*], Giribaskar Sivaswamy [a], M. Amir Siddiq [b], Alan Leacock [c], Paul Blackwell [d]

[a] Advanced Forming Research Centre (AFRC), University of Strathclyde, Glasgow, UK
[b] School of Engineering, University of Aberdeen, Aberdeen, UK
[c] Tirnaform Ltd, Carrickfergus, UK
[d] Department of Design, Manufacturing and Engineering Management, University of Strathclyde, Glasgow, UK

HIGHLIGHTS

- Repetitive Bending under Tension (R-BUT) testing was studied on how this mode of deformation affects material properties.
- Testing parameters had a significant impact on the uniform elongation and also on the required force to deform the samples.
- Depending on the R-BUT parameters, the increase in strain at fracture can be increased to 180% compared to tensile testing.
- FEA suggests that negative stress triaxiality under the R-BUT conditions explains the enhanced formability of samples.
- Conducting R-BUT testing leads to fine microstructure in the hexagonal structure Ti-50A sheets.

GRAPHICAL ABSTRACT

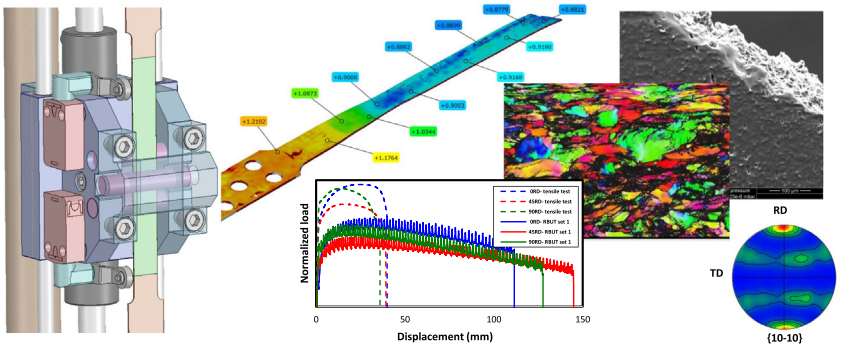

ARTICLE INFO

Article history:
Received 20 March 2020
Received in revised form 30 April 2020
Accepted 17 May 2020
Available online 19 May 2020

Keywords:
Repetitive bending under tension
Designing
Ti-50A
Microstructure
Formability
Fractography
FE analysis

ABSTRACT

The aim of this work was to study the cold formability of commercially pure Titanium alloy (Grade 2) by a testing methodology known as repetitive bending under tension (R-BUT). A dedicated test rig to perform the test was designed and fabricated to analyse the room temperature deformation behaviour of Ti-50A alloy sheet of 1.2 mm thickness. Samples from three different orientations were tested to investigate the effect of mechanical anisotropy on deformation behaviour. The results confirmed a significant increase in elongation to failure in samples subjected to R-BUT as compared to those subjected to standard tensile tests under similar conditions. This may be due to a delay in localised necking during R-BUT. Finite element analysis (FEA) suggested that a decrease in stress triaxiality in R-BUT could be the reason for enhanced formability of the materials compared to the conventional tension. Furthermore, electron backscatter diffraction (EBSD) study of the microstructure confirmed the development of highly strained regions that eventually lead to the formation of fine grains in the samples subjected to R-BUT. This could be due to a strain induced dynamic recovery process occurring during the test.

* Corresponding author.
E-mail address: saeed.tamimi@strath.ac.uk (S. Tamimi).

https://doi.org/10.1016/j.matdes.2020.108814

1. Introduction

Conventional sheet metal forming processes involve the cost of dies and long lead times which are not suitable for short term manufacturing activities. One method of avoiding high die costs and long lead times is to develop processes that do not involve dies. One such example includes incremental sheet forming (ISF). This rapid prototyping method comprises of a smooth tool fitted on a CNC milling machine that controls the movement of the tool in all three dimensions to form a part based on 3D-CAD data. Many researchers have performed experimental and numerical studies to better understand the process [1–6]. The deformation mechanism under the action of the forming tool in the ISF process has been investigated in the past and it was reported that high levels of straining and formability can be achieved during the process [7–10]. In order to better understand the deformation mechanics of ISF process, a rigorous effort has been made by proposing tests which may have similar loading and deformation behaviour [10,11]. One such test, known as repetitive bending under tension, is discussed in the following along with its relationship with ISF process.

The repetitive bending under tension (R-BUT) test was initially recommended by Benedyk et al. [12] to understand the deformation behaviour of sheet materials experiencing high levels of straining. In the case of R-BUT tests, the sheet metal sample is subjected to localised bending under tensile loading. This additional bending during testing is applied by sliding a set of rollers over the gauge length of the tested sample. Hu et al. [13] reported that the additional bending during R-BUT testing led to a significant drop in the magnitude of tensile load required for achieving the same amount of tensile elongation. Emmens et al. [14] have identified that the deformation conditions during the R-BUT test are similar to that of incremental forming processes where the sheet metal samples can be taken to relatively high strain levels before their fracture. The authors also noted that in the case of R-BUT, the sheet metal deforms incrementally when compared to standard tensile test where the sample deforms continuously. The relevance of this is that a sheet metal that is continuously being deformed will generally end up in localised failure due to the formation of voids leading to cracks and fracture. Hadoush et al. [15] reported that deformation of sheet materials between the rollers in the case of repetitive bending under tension is similar to that of the deformation of sheet material coming under the forming tool of an ISF process.

The incremental sheet metal forming process is a die-less method, which can form sheet metal parts of complex geometry using a CNC machine and a simple forming tool. It was introduced by Iseki et al. [16] as a flexible incremental sheet bulging process with the aid of spherical roller. The reason for referring to the process as ISF is due to the fact that at any instant in time only a localised part of the sheet metal blank is actually being formed. In this process, the sheet material workpiece is clamped rigidly around its edges with or without support underneath and formed using a tool with hemispherical tip at the forming end. Even though ISF is a slow process, many engineers want to adopt this method for small batch production. This is primarily due to the simple and cost-effective tools required to form a part having complex shape and geometry. In the case of ISF, depending on the process parameters, the strains imposed on the deforming sheet material are much higher than the strain predicted by their forming limit curves [17]. In addition, the sheet materials undergoing the ISF process are less prone to formation of localised necking in comparison with the sheet metals subjected to conventional sheet forming operations e.g. by deep drawing. Theoretical and FEM studies proposed that through-thickness and in-plane shear deformation occurring in the sheet metal subjected to ISF could be the reason for increased formability [18–20]. Sawada et al. [21] suggested the possibility of bending under tension as the prime reason for creating large stable deformation in the sheet material coming underneath the forming tool tip of ISF. This mechanism was proposed based on FEM simulation. However, in the case of ISF the stress field created in the sheet coming under the forming tip is fairly complex and may include double bending [14]. Repetitive bending during tensile loading has been suggested as a method of developing an understanding of the mechanisms behind the deformation characteristics of sheet metals during ISF [22]. The set of rollers used in the R-BUT test act in a similar way to the tool used in ISF to generate localised deformation. There remain a number of questions to be answered to develop a fuller understanding of why sheet materials show enhanced formability when subjected to repetitive bending under tension and the effect of such deformation on crystallographic texture. The influence of through-thickness shear plastic deformation and strain path changes on microstructure evolution of steel sheets have been studied [23]. Zecevic et al. [24] claimed that a delay in ductile fracture led to the formation of a strong <111> fibre texture in the case AA-6022-T4 alloy subjected to R-BUT. Weakening of texture in the case of AZ31 Magnesium alloy after repetitive bending under tension has been reported by Yang et al. [25].

In this study, a novel test rig has been designed and fabricated to perform repetitive bending under tension to investigate the formability of commercially pure titanium grade 50A (Ti-50A). Due to interest from industrial partners in the formability of commercially pure titanium grade 50A, this material was chosen as the subject for the investigation. This paper aims to present a clear understanding of the room temperature formability of this alloy when subjected to R-BUT, and its dependency on process parameters such as strain rate by varying the roller velocities. Design aspects of the test rig used in this study are also presented and discussed. Effort has been made to analyse the changes in the microstructure as well as changes in crystallographic texture occurring in the samples subjected to the R-BUT test. The scanning electron microscopy (SEM) based electron back scattered diffraction (EBSD) technique was used for textural investigation and a 3D scanning technique was utilised to analyse dimensional changes occurring in the tested samples after R-BUT and normal tensile tests. Effect of R-BUT process parameters are also simulated using finite element methods and new insights on the deformation and failure mechanism has been presented.

2. Experimental procedure

2.1. Material and processing

The materials used for this investigation was commercially pure titanium grade 2 (Ti-50A) with 1.2 mm thickness, and a nominal chemical composition provided in Table 1. For the R-BUT experiments, a testing frame comprising of a movable three-point bending roller assembly, sample holders and power supply were designed and manufactured. The mobile three-point bending assembly consisted of 3 rollers equally spaced at 35 mm along the lengths of the sample such that the middle roller (which generated the bending) was able to travel along the full gauge length of the sample taking into consideration the gauge length extension and maximum deformation percentage during the test – see Fig. 1. The level of bending was controlled by adjusting the position of the central roller. All the rollers were cylindrical with 15 mm diameter, made from hardened tool steel.

The bending fixture was integrated into a screw driven Zwick/Roell Z150 standard mechanical testing machine, such that the upper and lower grips of the tensile machine were aligned with the longitudinal direction of the sample. For the application of uniform bending along the gauge lengths of the specimens, appropriate housings were manufactured to accommodate the rollers and the sample during the test. As the length of the sample increased during the test, the gauge

Table 1
Nominal chemical composition of Ti-50A alloy (wt%).

O	N	C	Fe	H	Ti
0.25	0.03	0.08	0.30	0.015	Remaining

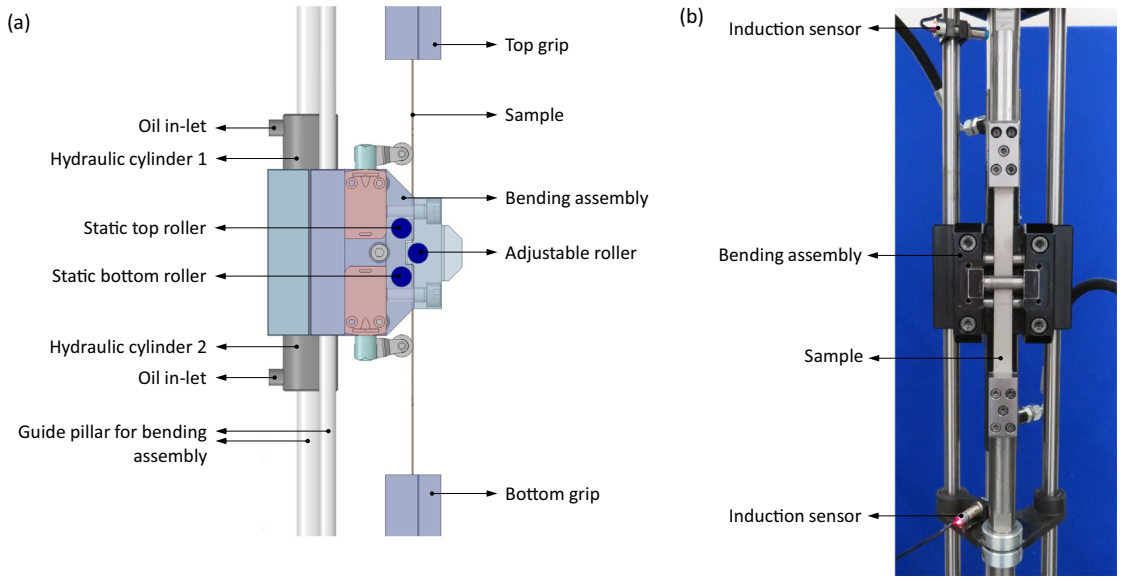

Fig. 1. Repetitive bending under tension testing assembly: (a) CAD model showing the side view of the test rig illustrating the sample and important parts of the fixture and (b) photographs showing the actual test rig fitted to a mechanical testing machine (Zwick/Roell Z150) used for this study.

length (i.e. deformation zone) also continuously increased until the final failure. Two pneumatic cylinders powered by a hydraulic motor were designed to provide the driving force to operate the bending assembly along the gauge length of the specimen with a vertical reciprocating motion. This was controlled by setting upper and lower limits for the roller's assembly oscillation using a pair of induction sensors that were fixed on either side of the sample gauge length. The induction sensors detected the limits of the roller motion on both ends of the gauge length and by sending signals back to the direction control valves of the power supply, the direction of the bending assembly motion was altered. The induction sensors were adjusted by the extension of the tensile testing grip during the test. The vertical speed of the bending assembly was controlled using flow control valves on the hydraulic power supply. Minimum and maximum achievable speeds for the assembly were between 20 and 80 mm/s, respectively.

The geometry of the tensile specimens used in this study was adopted from ASTM standard for sheet, strip, flat wire and plate [26]. The geometry and dimensions of the R-BUT and tensile testing samples are presented in Fig. 2. The sample dimensions have been scaled up to provide sufficient space to accommodate the bending assembly and its domain of oscillation during the test. Therefore, samples with total length of 320 mm and gauge length of 200 mm were designed and manufactured. The maximum level of elongation in the gauge length achieved during these tests was 120 mm, or 60%.

The setup of a typical repetitive bending under tension test included three steps of (i) clamping the sample on the tensile machine and aligning the sample with the roller assembly, (ii) bending the sample in the roller assembly to a specified bending value while the tensile machine was in load control mode to keep the load at 0 N, and (3) once the specified level of bending was achieved then the sample was loaded in tension and the roller assembly started to oscillate and applied the localised bending to the gauge length, simultaneously. The oscillation frequency of the R-BUT tests is a function of bending velocity. For the bending velocities of 7, 20 and 80 mm/s (as used in these tests), the frequencies are 0.025, 0.08 and 0.25 Hz, respectively. All experiments were carried out at ambient temperature at a crosshead displacement of 0.2 mm/s that was approximately equivalent to a strain rate of 10^{-3} s^{-1}.

A range of tests was developed to investigate the influence of the major experimental parameters; including the level of bending and the travel speed of the bending assembly along the sample gauge length. These conditions were investigated on three batches of samples with their lengths parallel to RD (0RD), at 45° to RD (45RD) and perpendicular to RD (90RD), respectively, to study the influence of the material's mechanical anisotropy. These are all summarized in Table 2. Additionally, a set of standard tensile tests, without the application of the repetitive bending, were carried out on each sample orientation, for the purpose of comparison.

2.2. Microstructure characterisation

Scanning electron microscopy and electron backscatter diffraction was used for microstructural characterisation. For these analyses, samples with approximate dimensions of 8 mm × 15 mm were cut from the as-received sheet, and from the samples after a standard tensile test as well as from samples following repetitive bending under tension. Samples were taken in the plane parallel to the rolling direction (RD), and mechanically ground and polished to a mirror finish. The polished finished samples were then subjected to a final stage of electro-

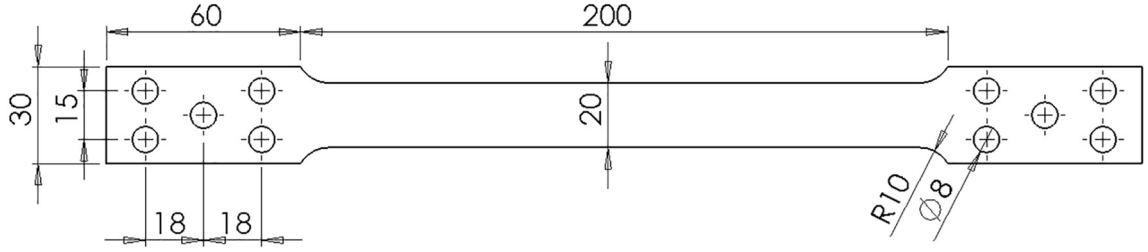

Fig. 2. Geometry and dimensions of the sample used for repetitive bending under tension test. All dimensions are in mm.

Table 2
Different repetitive bending under tension test setting.

Configuration	Roller penetration (mm)	Bending assembly speed (mm/s)	Pulling speed in tension (mm/s)
Set 1	1.25	20	0.2
Set 2	4	20	0.2
Set 3	1.25	80	0.2
Set 4	4	80	0.2
Set 5	0.88	7	0.2
Set 6	0.88	20	0.2
Set 7	0.00	0.00	0.2
Set 8	4	0.00	0.2

Table 3
Study of increase/decrease in uniform elongations and forces of repetitive bending under tension with different roller penetrations in comparison with normal tensile testing.

Bending level	% increase in strain at fracture	% decrease in max force
	Reference	Reference
0.00		
	140%	16%
0.88		
	180%	24%
1.25		
	105%	65%
4		

polishing to remove approximately 20–30 μm material from the mechanically polished surface using Struers electrolyte A2 at ambient temperature for 45 s at 35 V. The acquisition of EBSD maps was carried out using a fully automated AZtec HKL Advanced (plus C5 Prem) Nordlys Max 2 EBSD system interfaced to a FEI Quanta-650 field-emission gun scanning electron microscope, with an accelerating voltage of 20 kV and a 100 μm diameter aperture. The acquisition time was set to 40 ms, collecting at least 2 frames for each point. Orientation mapping was performed on the sample cross sections with 0.3 μm step size. In all cases, a minimum of 70% of the scanned areas were indexed. In addition to the microstructure characterisations, the fracture surfaces of tested samples were investigated by SEM to understand the mode of fracture and assess any void formation.

2.3. Thickness reduction measurements

A non-contact blue light 3D scanning technique was adopted to analyse the changes in the thickness along the gauge section of the samples before and after the tests with the aid of A GOM ATOS® software. The primary objective of these measurements was to explore the uniformity of thickness reduction along the gauge length throughout the R-BUT tests in comparison to the standard tensile test. Initially the sensor unit of the ATOS system projects different fringe patterns on the samples to be measured and records them via two cameras. Then the 3D coordinates for each camera pixel are calculated with high precision based on the optical transformation equations. A photogrammetric methodology is used for the geometrical configuration of the system. Transformation into a global coordinate system is performed automatically by means of the reference points. Each individual measurement completes the building-up of the 3D model of the scanned sample which can be used to determine thickness reduction to an accuracy of 5 μm [27].

Table 4
Tensile properties of Ti-50A alloy derived from the uniaxial tensile test done on 0RD sample.

Modulus of elasticity (GPa)	Yield strength (MPa)	Tensile strength (MPa)	Strain at UTS
137	324	455	0.17

3. Results

3.1. Repetitive bending under tension of Ti-50A

In this section, the influence of repetitive bending under tension on the mechanical behaviour of Ti-50A samples is discussed based on the load-displacement curves derived at different roller penetration depths. Note that an increase in penetration depth increases the amount of bending which in turn decreases the bending radius in the deformation zone. The load-displacement curves derived from the tests conducted at different roller penetration depths are given in Fig. 3(a). For comparison, this includes the load-displacement curve from a simple tensile test (see also basic tensile data given in Table 4). It may be seen that roller penetration depth has a significant impact on the deformation characteristics of the samples tested at the same engineering strain rate. It was apparent that higher penetration depths resulted in lower maximum loads taken by the sample before it fractured. Also, there was a noticeable increase in the value of maximum displacement by the samples subjected to repetitive bending under tension as compared to the sample subjected to simple tension. The maximum displacement was found to increase when the penetration depth was raised from 0.88 mm to 1.25 mm, which is shown by the load-displacement curves given in blue and red colours, respectively. As the roller penetration

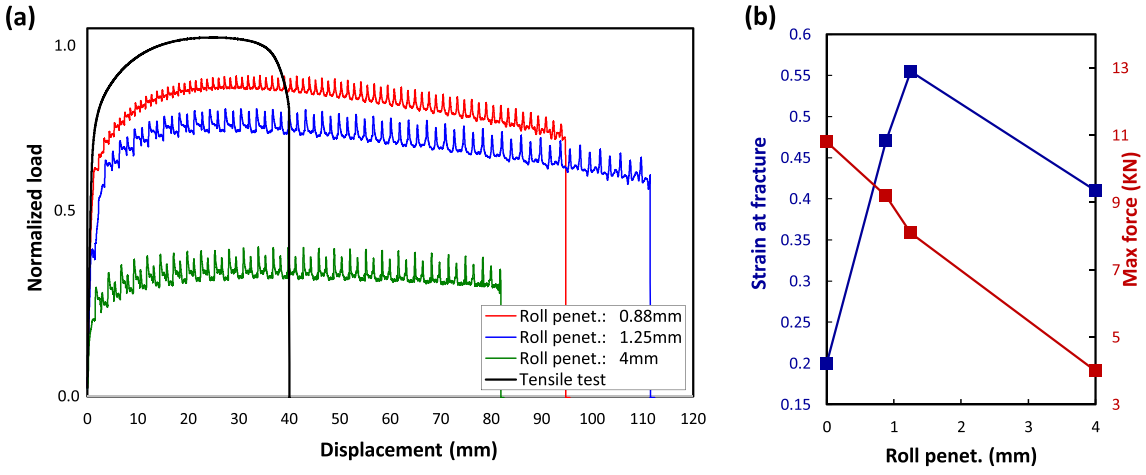

Fig. 3. Effect of bending level on the mechanical response of Ti-50A alloy during repetitive bending under tension testing: a) load-displacement and b) corresponding strain at fracture and maximum force of each condition.

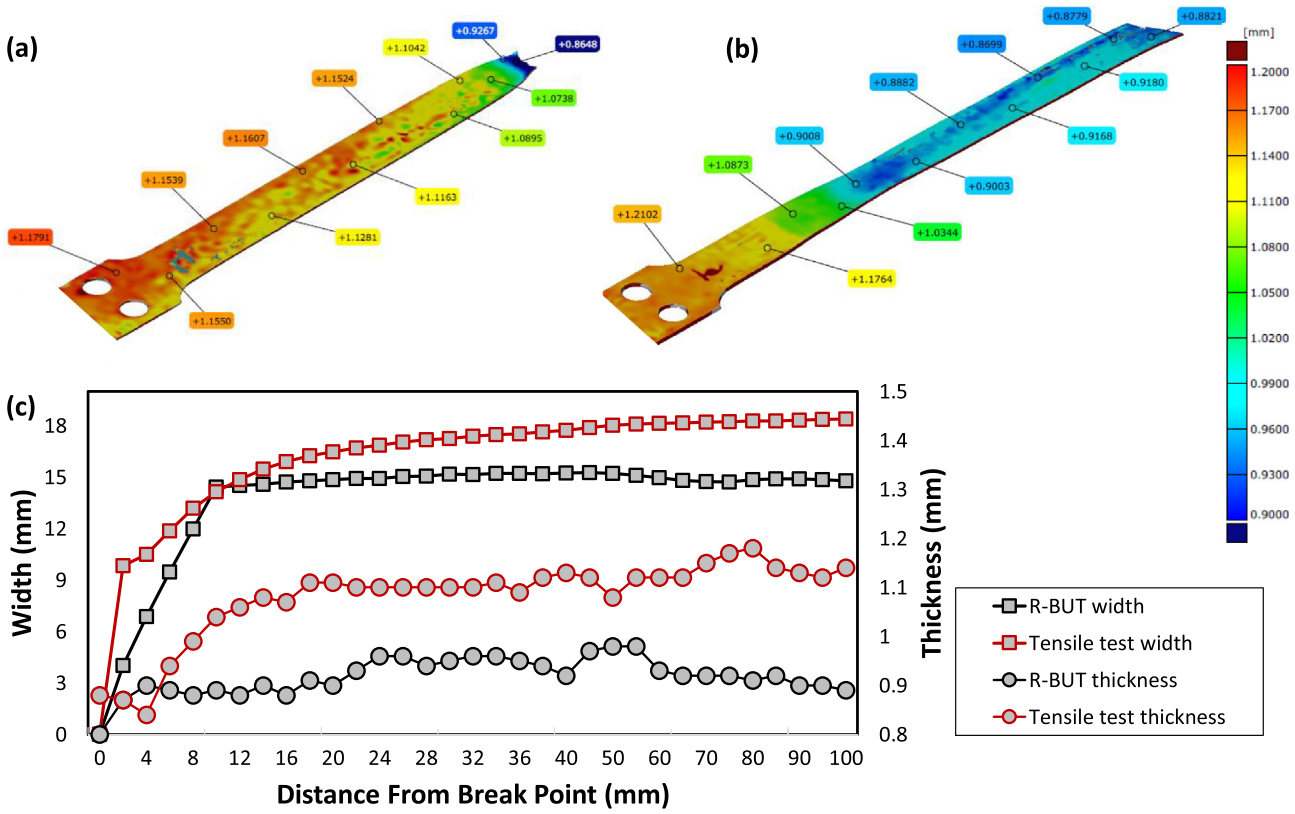

Fig. 4. 3D scanning results showing the variation in the thickness in the case of samples subjected to (a) tensile testing and (b) repetitive bending under tension testing; (c) Graphical representation of changes in the values of thickness and width of samples from the fracture tip after the tests.

depth increases, the material requires less pulling force with a decrease in the bending radius to undergo deformation during repetitive bending under tension. However, a further increase in the depth from 1.25 mm to 4 mm led to a decrease in the value of maximum displacement taken by the sample which is shown by the load-displacement curve in green.

The effect of roller penetration depth on the fracture strain is also shown in Fig. 3(b). Strain at fracture was calculated by considering the length of the tested samples before testing and after testing. The data, including the percentage changes in maximum force, is tabulated in Table 3.

The basic mechanical properties of Ti-50A from the standard uniaxial tensile test along the rolling direction are given in Table 4.

Surface colour plots from the scanned samples showing the thickness and width variations of one of the SET 2 test pieces together with a simple tensile test are given in Fig. 4(a) and (b). The colour coded bars with thickness values give information about the percentage reduction in thickness as well as width along the gauge section of the scanned samples. It will be noted that the width of the gauge section in the case of tensile tested samples remained relatively stable whereas the R-BUT samples demonstrated a noticeable, but uniform reduction along the gauge width. Samples subjected to R-BUT testing exhibited gradual reduction in thickness during testing whereas in the case of samples subjected to tensile testing, the thickness remained constant outside of the necked zone. Overall, this is suggestive of more stable flow of the material under the R-BUT conditions.

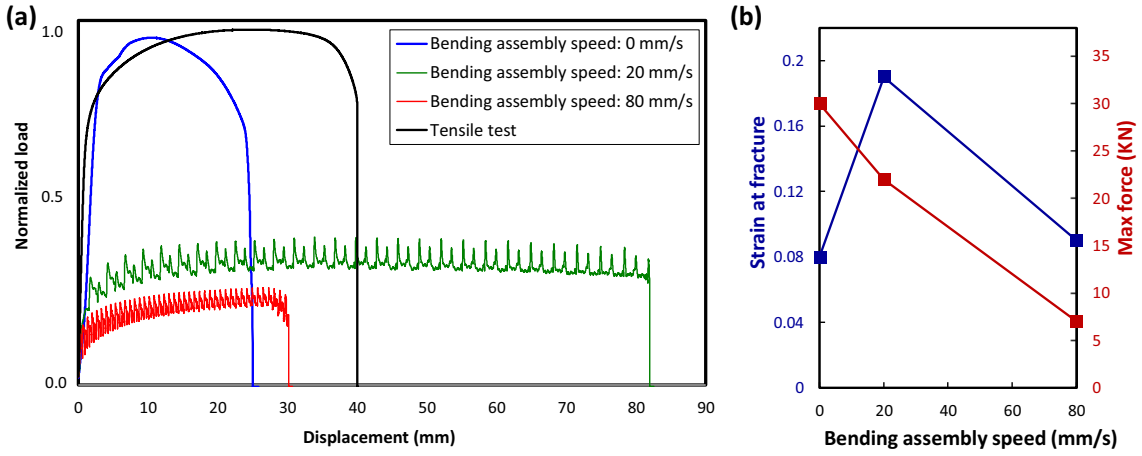

Fig. 5. (a) Comparison between the load-displacement curves for a normal tensile test and for repetitive bending under tension tests done by varying the speed of bending assembly. (b) Effect of speed of bending assembly on the value of maximum force attained and on the values of fracture strains by the tested samples of 0RD orientation.

Table 5
Study of increase/decrease in uniform elongations and forces of repetitive bending under tension with different bending assembly speeds in comparison with normal tensile testing curve.

Bending assembly speed (mm/s)	% change in fracture strain	% decrease in maximum force
0.00	Reference	Reference
20	105% ↑	65%
80	25% ↓	79%

Table 6
Amplitude of peaks-troughs for different penetration depths.

Penetration depth (mm)	10%	30%	60%	80%
0.88	0.35	0.45	0.65	0.7
1.25	0.55	0.6	0.65	0.7
4	0.9	0.85	0.8	0.8

Fig. 5 shows the effect of the velocity at which the bending assembly moves upward and downward along the gauge length. For these tests the bending radius, which is a function of the penetration depth was maintained constant (4 mm was used here). The figure shows that an increased speed of travel of the roller housing from 20 to 80 mm/s decreased the uniform elongation and also the force required for deformation. The black curve represents the load-displacement curve of a simple monotonic tensile test while the blue curve denotes the behaviour seen during a tensile test with the assembly remaining static. Note that sample geometry used for both test scenarios was similar as shown in Fig. 2. The maximum force recorded for both cases are more or less equal to 10.5 kN though the elongation and yield strength for the tensile result was higher.

Note that in both cases, the samples were tested up to fracture. The overall results are summed up in Table 5.

The serration with peaks and troughs seen on the load – displacement curves of the samples given in Fig. 3(a) is associated with change in the direction (upward and downward movements) of the roller movement during the tests. Four displacement values are considered for analysing the peaks and troughs appearing in the load-displacement curves which are indicated by dotted rectangular boxes in the figure. The values from this are given in Table 6. The amplitude was found to gradually increase for the case of 0.88 mm to 1.25 mm penetration depths. But in the case of 4 mm penetration, the amplitude of peaks and troughs is fairly high from the beginning of plastic regime.

3.2. Anisotropy in repetitive bending under tension testing

The mechanical responses of Ti-50A to repetitive bending under tension and tensile tests along 0RD, 45RD and 90RD are shown in Fig. 6. All the repetitive bending under tension tests were carried out using a constant bending assembly speed of 20 mm/s and a bending level of

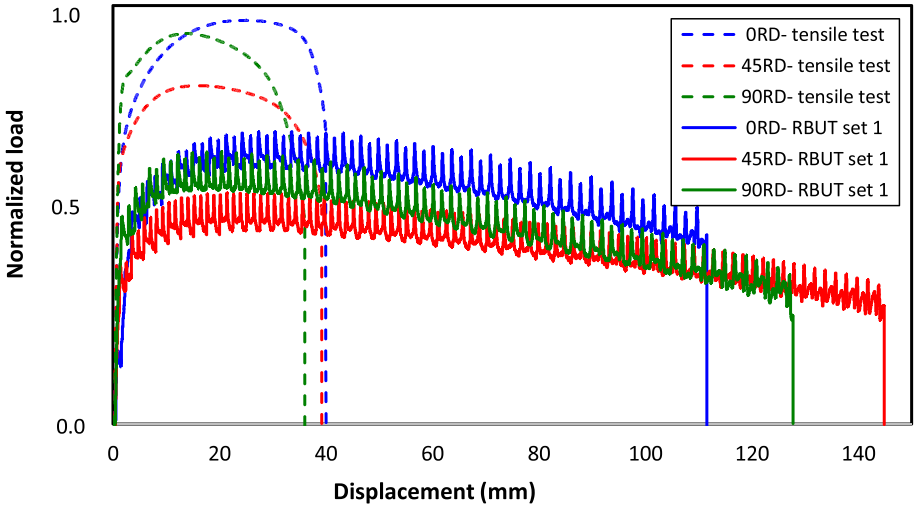

Fig. 6. Effect of anisotropy on the behaviour of Ti-50A alloy subjected to repetitive bending under tension tests.

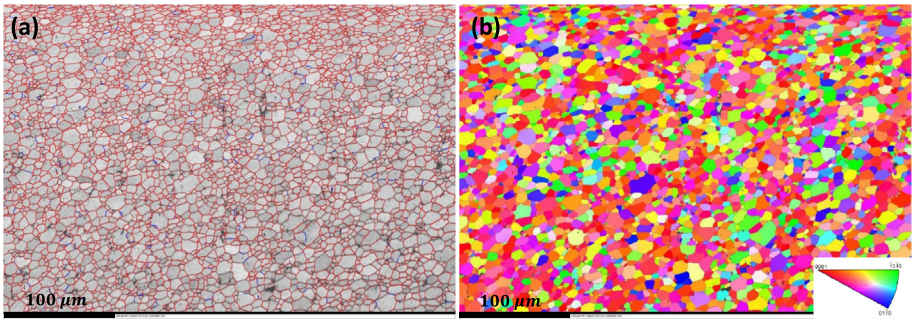

Fig. 7. EBSD results from RD-TD plane of the as-received material: (a) grain boundary map superimposed on image quality map, (b) inverse pole figure map.

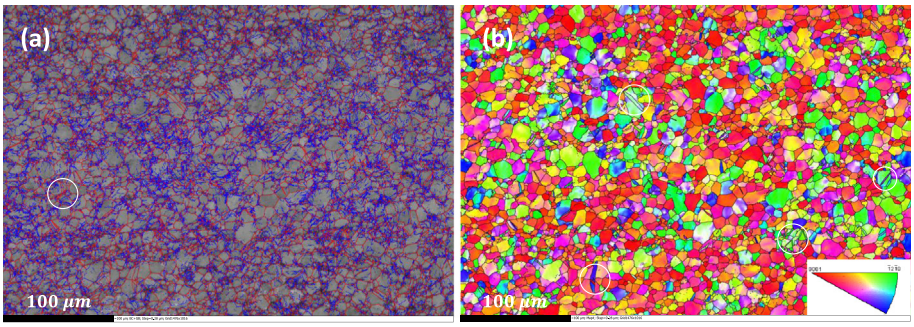

Fig. 8. EBSD results from RD-TD plane of the tensile tested sample showing the evidence for deformation twins (indicated by circles) and fragments of low angle boundaries (blue) with- in the pre-exiting grains surrounded by high angle boundaries (red): (a) grain boundary map superimposed on image quality map, (b) inverse pole figure map.

1.25 mm. The pulling speed of the tests was kept constant at 0.2 mm/s which approximately translated to 10^{-3} s^{-1} engineering strain rate. The Lankford coefficient of Ti-50A which was obtained from the tensile tests along 0^0, 45^0 and 90^0 from the RD was approximately, 1.1, 2.4 and 1.8, respectively.

The results indicate that, samples along 45RD (i.e. red curves in Fig. 6) show higher formability than other directions. In addition, the maximum force for the 45RD samples was below that of 0RD and 90RD. This could be due to the lower material strength along 45RD compared to the other directions. In terms of hardening behaviour, the R-BUT results show less sensitivity to the test direction than the monotonic tensile test curves. In other words, although material under tension along 0RD has a higher hardening rate than other directions, in repetitive bending under tension testing along 0RD the material deformed with a similar hardening rate as 45RD and 90RD. This indicates that deformation mechanism under repetitive bending under tension might be different than that in tensile test. This could be associated with different twin-slip system activities

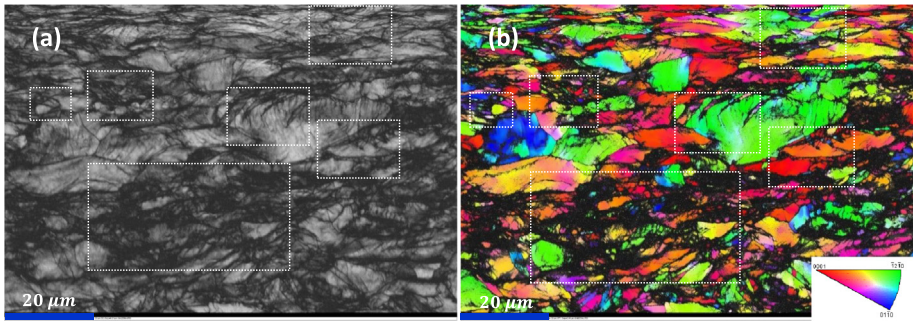

Fig. 9. EBSD maps from RD-TD plane of the sample after R-BUT test showing the evidence for the formation of fine grains in the matrix: (a) image quality map and (b) image quality map. Dotted rectangles indicate the regions having fine grains.

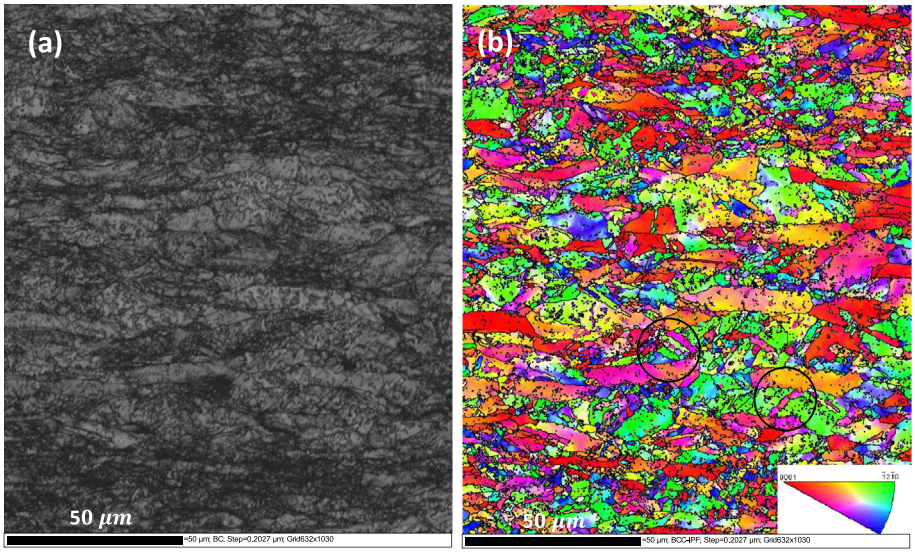

Fig. 10. EBSD maps from the RD-ND plane of the sample subjected to R-BUT showing the evidence for the formation of deformation twins and fine grains within the pre-existing grains in the matrix: (a) IQ map and (b) IPF map.

during cyclic loading when compared to the monotonic tensile loading [28,29].

3.3. Microstructure analysis

EBSD results showing the microstructural characteristics of the as-received material are shown in Fig. 7. The image quality map superimposed by a grain boundary map in Fig. 7(a) confirms that majority of grains are surrounded by high angle grain boundaries. Red colour lines are used to indicate high angle grain boundaries (HAGB) and low angle grain boundaries (LAGB) are marked by blue coloured lines. Fig. 7(b) is the inverse pole figure map showing the presence of equi-axed grains having a random orientation. Orientation of individual grains in the matrix can be identified by the colour coded inverse pole figure shown. These maps confirmed the absence of deformation twins within the grains in the alpha phase matrix. Note that EBSD scan was done on the RD-TD plane.

Results from EBSD scan on the RD-TD plane of samples after tensile testing are given in Fig. 8. It is noted that pre-existing grains in the matrix have not lost their equi-axed morphology under tensile load. But evidence for formation of grain boundary segments (blue colour), which are mostly low angle in nature, was observed in the grain boundary map given in Fig. 8(a). Also formation of twin boundaries as a result of tensile loading within the pre-existing grains was observed in this case. The IPF map given in Fig. 8(b) shows deformation twins with in the matrix (marked by white circles). The RGB colour code: red for (0001), green for ($1\bar{2}10$) and blue for ($01\bar{1}0$) as shown in the standard stereographic triangle; corresponds to the crystallographic orientation of each grain. Many grains exhibited minor misorientation differences with in the grain interior.

The EBSD results shown in Fig. 9 reveal the formation of sub-grains within the pre-existing grains in the case of samples subjected to repetitive bending under tension testing. Dotted rectangular boxes marked in the image quality map show the regions having fine grains in the matrix (Fig. 9(a)). Such grains may be the result of dynamic recovery occurring during repetitive bending under tension. The IPF map given in Fig. 9 (b) confirms the formation of sub-grains was likely produced as a result of dynamic recovery processes.

The results of an EBSD scan carried out on the RD-ND plane of a sample that underwent repetitive bending under tension testing is given in Fig. 10. The IQ map given in Fig. 10(a) confirms the presence of highly strained regions within the elongated grains in the matrix. The IPF

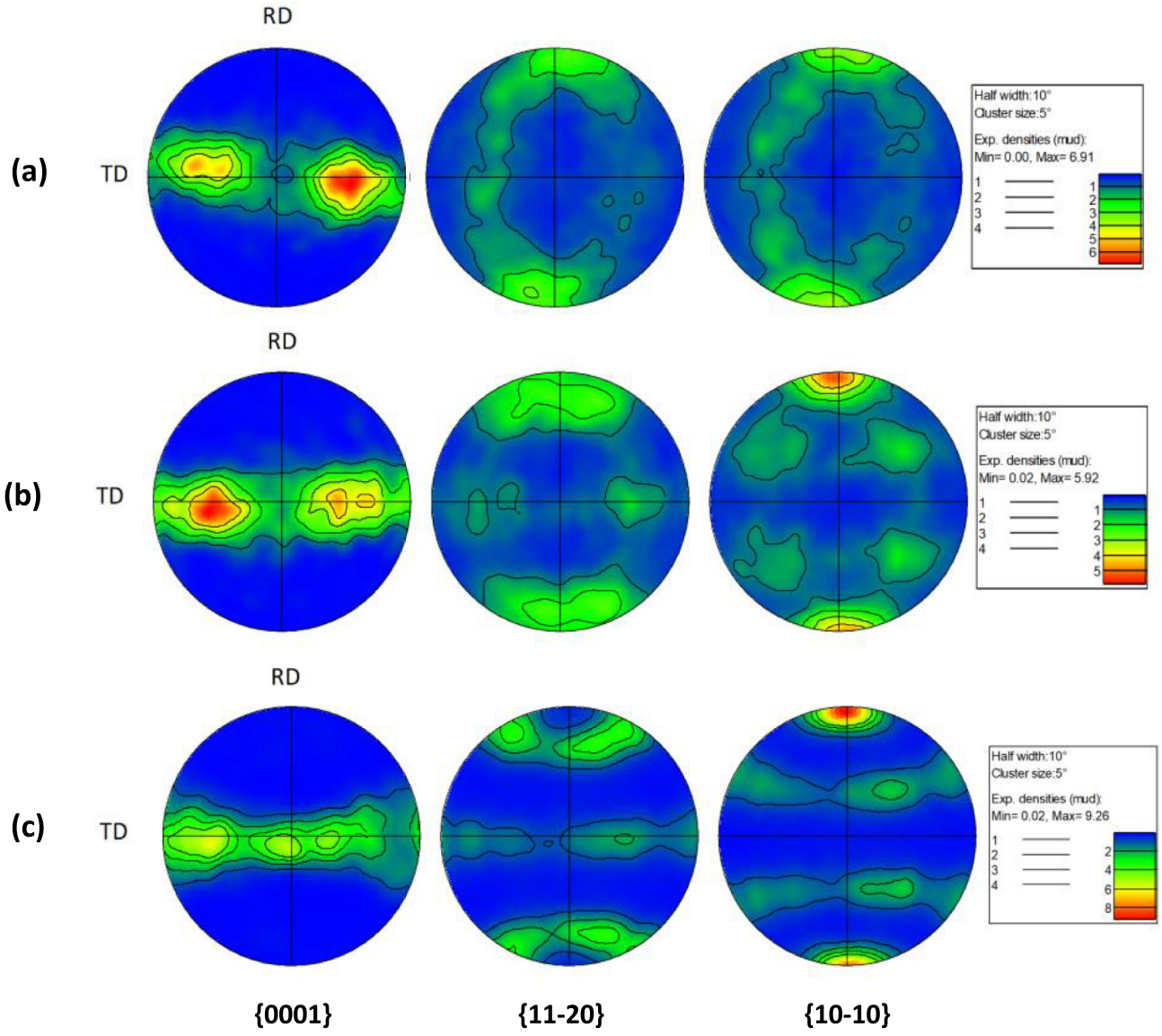

Fig. 11. Experimentally measured pole figures showing the evolution of texture on basal (0001), prismatic ($10\bar{1}0$) and pyramidal ($11\bar{2}0$) planes of the Ti-50A: (a) as-received, (b) after tensile testing and (c) after repetitive bending under tension testing. The colour scale bar for the corresponding pole figures representing the texture intensities are given as inserts.

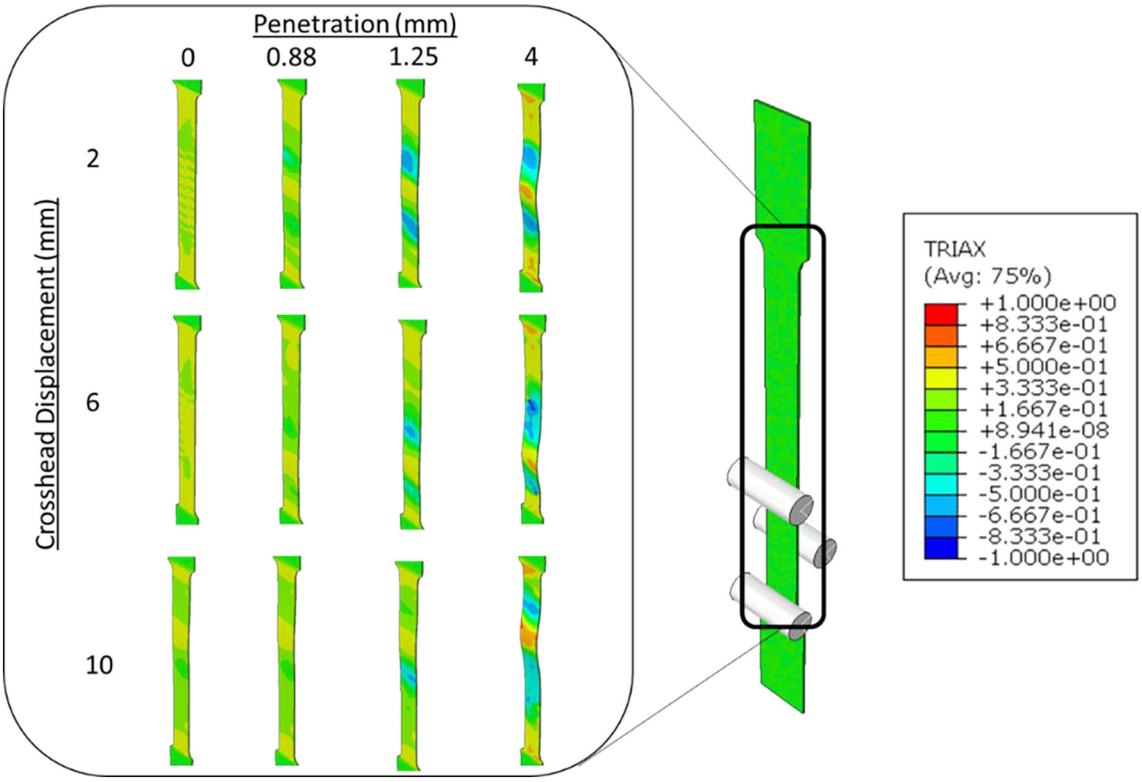

Fig. 12. Evolution of stress triaxiality for different roller penetration depths and deformation stages for 0RD orientation sample.

map given in Fig. 10(b) shows the formation of deformation twins within the pre-existing grains of the α phase. There are locations where the twinned areas are subdivided into smaller and smaller features surrounded by high angle boundaries (see marked circles). This could be due to the accumulation of dislocations due to slip activity in and around the twin boundaries during repetitive bending under tensile loading. Evidence for formation of fine grains within the elongated grains is also seen in the IPF given in Fig. 10(b). It should be noted

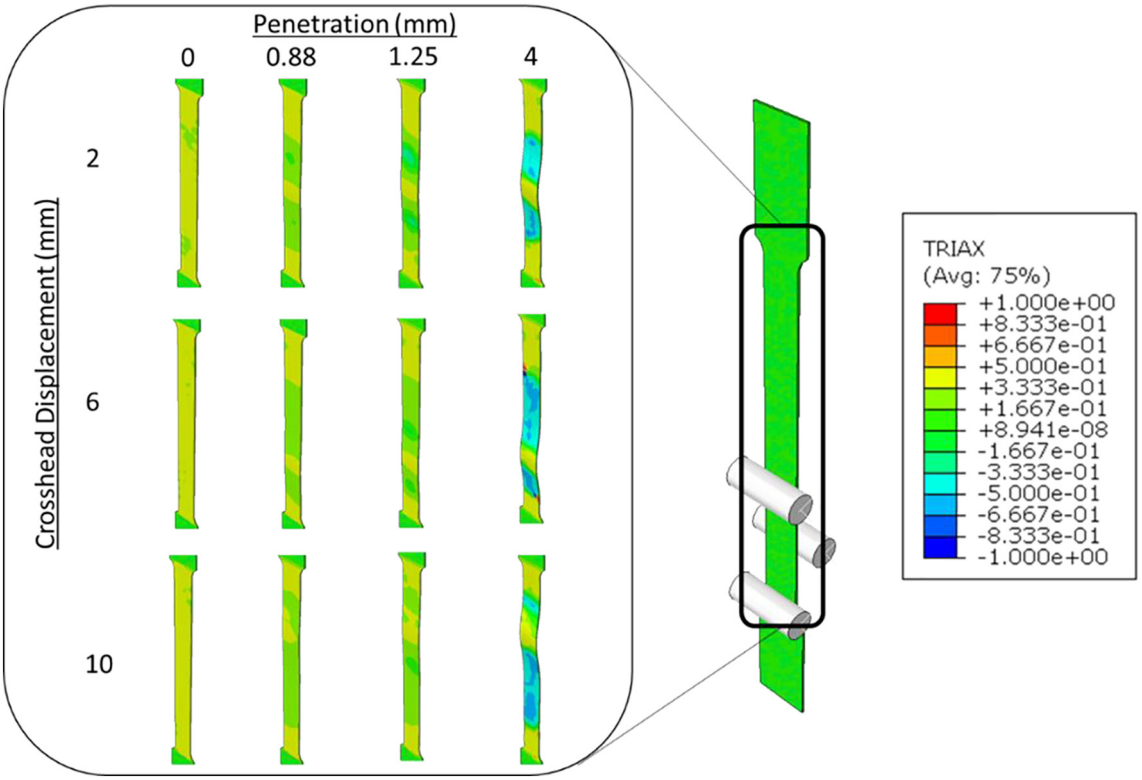

Fig. 13. Evolution of stress triaxiality for different roller penetration depths and deformation stages for 45RD orientation sample.

that the microstructure evolution through the sheet thickness direction was different. Due to the bending/unbending occurring during testing, the areas near to the sample surfaces experienced compression and tension as compared to the areas in and around the neutral axis, which is in middle of the sample tested. This leads to a difference in the level of deformation occurring to the pre-existing grains at the near surface as compared to the central zone.

3.4. Analysis of crystallographic texture before and after testing

Fig. 11(a)–(c) shows the experimentally measured pole figures describing the evolution of crystallographic texture on basal (0001), prismatic ($10\bar{1}0$) and pyramidal ($1\bar{1}20$) planes of the Ti50A alloy sample in the as-received condition, after tensile testing and after repetitive bending under tension testing, respectively. From the colour scale bars provided for each condition, it is confirmed that there is a reduction in texture strength after tensile testing and an increase in the texture strength after repetitive bending under tension test. The {0001} pole figures from the as-received condition (Fig. 11(a)) and after tensile testing (Fig. 11(b)) indicate that the c-axis is mainly oriented in the ND-RD plane and there were two peaks along the direction inclined to 50° from ND to RD (RD- split basal texture). However, after repetitive bending under tension the strength of those peaks came down. This was associated with the weakening of split-basal texture which is displayed by the {0001} pole figure shown in (Fig. 11(c)). Evidence for formation of a basal ND texture due the formation of grains with the c-axis parallel to the normal direction of sheet sample with the spread of 15–20° is also shown by the {0001} pole figure given in (Fig. 11(c)). The pyramidal {$1\bar{1}20$} and prismatic {$10\bar{1}0$} pole figures of the samples after tensile testing showed the formation of the <$1\bar{1}20$> and <$10\bar{1}0$> fibres (Fig. 11(b)). Moreover {$10\bar{1}0$} pole figure from Fig. 11(b) showed the intensity of prism poles getting strengthened after tensile testing.

3.5. Finite element analyses of R-BUT

In order to get a better understanding of the deformation mechanics of the Ti-50A alloy during the R-BUT test, a three-dimensional finite element (FE) model was constructed in ABAQUS. The sample had the same dimensions as used in the experiments (Fig. 2). Ti-50A material was defined using Hill's anisotropic yield criteria with material parameters identified through experiments (for details see [30]). The R-BUT tests were simulated for 4 different roller penetrations, i.e. 0 (conventional tensile test), 0.88 mm, 1.25 mm, and 4 mm. Also, two orientations of Ti-50A, viz. 0RD and 45RD were simulated. Figs. 12 and 13 show the plot of stress triaxiality for different roller penetrations and deformation for 0RD and 45RD. The FE model is able to capture the effect of sample orientation with different triaxiality distributions for 0RD and 45RD. It can be inferred from Figs. 12 and 13 that for the case of penetration = 0 mm, i.e. a conventional uniaxial test, the stress triaxiality remains around 0.33, which is generally the case for uniaxial loading. However,

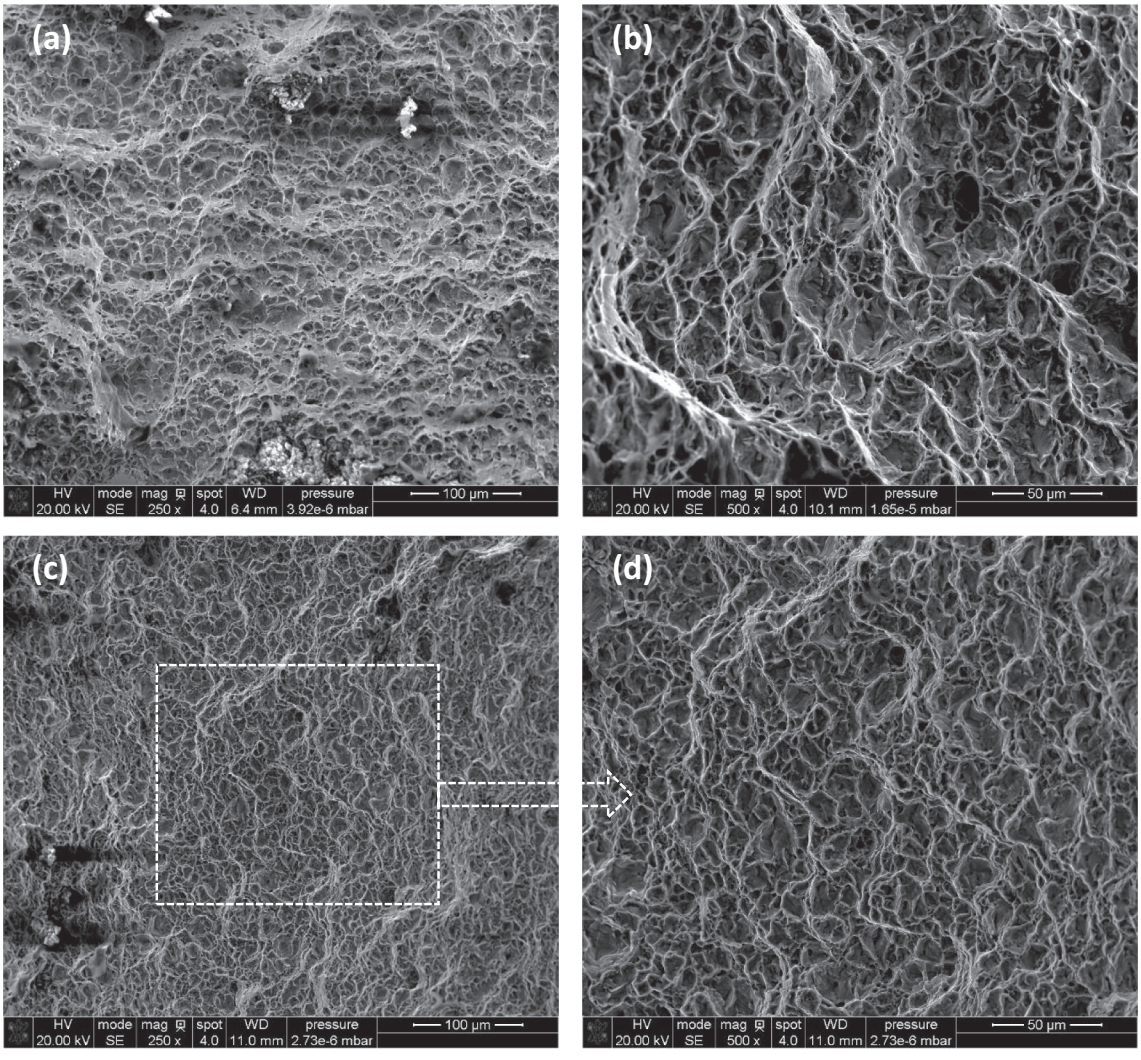

Fig. 14. Secondary electron images showing the characteristics of fracture surfaces in the case of tensile testing ((a)&(b)) and repetitive bending under tension test ((c)& (d)).

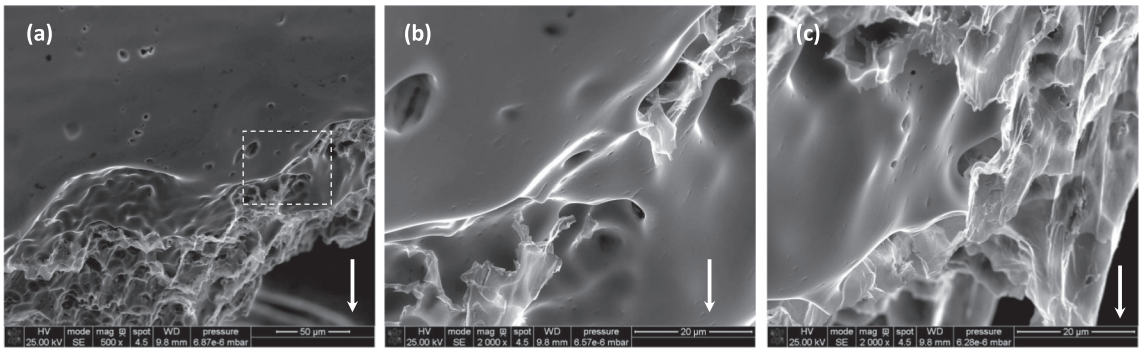

Fig. 15. SEM–SE micrographs of different magnification showing the evidence for formations of voids and micro-voids close to the fracture tip in the case samples subjected to simple tensile test (white arrow indicates the load direction).

for the case of non-zero penetrations, such as 0.88, 1.25, and 4 mm, it was found that stress triaxiality is non-uniformly distributed and the contact areas right under the rollers show negative triaxialities. The plots also show that the regions of negative and positive stress triaxialities move with the roller for the three different deformation stages, i.e. at a crosshead displacement of 2, 6, and 10 mm. It can further be seen from Figs. 12 and 13 that as the penetration is increased the value of negative triaxiality increases.

3.6. Fractography

Fracture surfaces of the samples that went up to fracture in the case of tensile testing (Fig. 14(a), (b)) and repetitive bending under tension (Fig. 14(c), (d)) were analysed by recording using secondary electron (SE) images. Although the mode of fracture that occurred in both cases was predominantly ductile fracture, the size of the dimples generated in the process of fracture was slightly different. The dimples are formed as a result of nucleation, growth and linking of voids prior to fracture. In the case of repetitive bending under tension the dimples formed were comparatively smaller than in the case of tensile tested samples. The size and morphology of the dimples formed in the case of repetitive bending under tension are shown in the low and higher magnification images from a selected area. The difference in dimple size may be due to differences in the stress state and strain path history which will directly influence the rate of void nucleation as well as the growth process during loading. In addition to that, the lower magnification image from the tensile tested sample shows dimples having a shallow depth at different location (Fig. 14(a)). This is suggestive of the fact that the tensile samples offered less resistance to deformation.

Evidence for formation of voids under the influence of a tensile load close to fracture is shown in the secondary electron images provided in Figs. 15 and 16. It is understood that ductile fracture occurring during tensile tests as a result of a large amount of plastic deformation consists of three important stages namely (i) void nucleation, (ii) void growth and (iii) void coalescence. Higher magnification images recorded close to the fracture tips of samples subjected to normal tensile tests and repetitive bending under tension revealed void coalescence occurring under the influence of tensile loads. Also formation of micro-voids close to the fracture zone is indicated from the higher magnification micrographs. These micro-voids are expected to form after necking under uni-axial tensile force which then undergo coalescence to form the crack, which is then expected to propagate in the direction more or less perpendicular to the tensile loading.

4. Discussion

The main objective of this study was to gain an in-depth understanding of the behaviour of Ti-50A sheet under repetitive bending under tension conditions. It was shown that the uniform elongation obtained by the R-BUT test was markedly enhanced in comparison with the samples subjected to tensile testing as shown in Figs. 3 and 5. The reason for such a significant increase in the displacement values is due to the stabilization of material flow that is generated by the repeated bending in the R-BUT test. Fig. 17 shows the photographs of the samples that went up to fracture under simple tension and repetitive bending under tension (penetration depth 1.25 mm). Fracture occurred in the samples subjected to simple tension as a result of diffuse necking followed by immediate localised necking occurring in the region of stress concentration within the gauge section (indicated by red dotted rectangle in Fig. 17(a)). The diffuse necking may terminate in fracture due to the formation of a narrow band (at an angle of approximately 54° to the axis of loading) the width of which is approximately equal

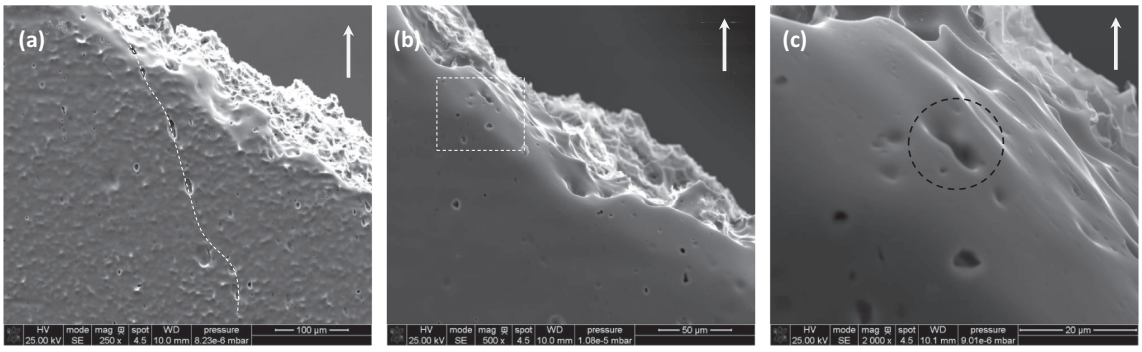

Fig. 16. SEM-SE images showing the formation of voids close to fracture tip in the case samples subjected to R-BUT: (a) series of voids forming along the grain boundary (indicated by dotted lines). (b) and (c) showing the evidences for void growth leading to void coalescence close to fracture tip. White arrow indicates the load direction.

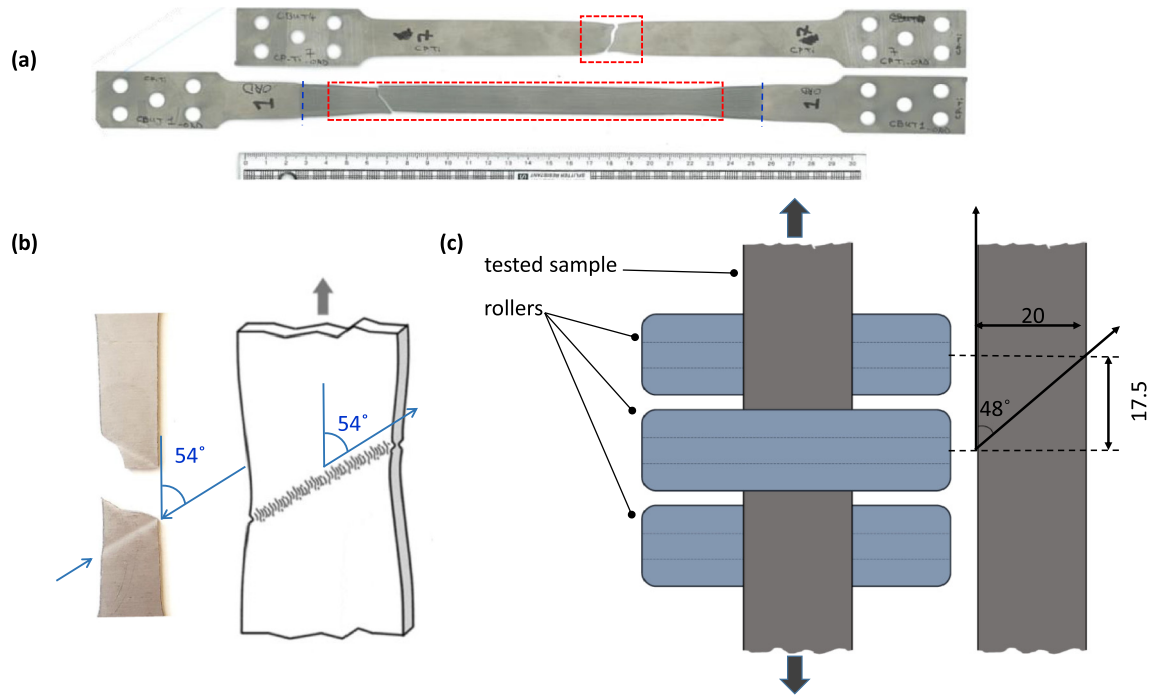

Fig. 17. Photograph showing the evidence for occurrence of progressive diffused and localised necking along the gauge section. (a) Photograph showing sample subjected to simple tension and repetitive bending under tension, (b) formation of band at an angle of 54° as a result of localised necking in the case of a sample subjected to simple tension. (c) A schematic of repetitive bending under tension showing the geometrical condition preventing the localised necking.

to the thickness of the sample. Note that these bands were clearly seen close to fracture tip of the samples that have undergone cup and cone type fracture during simple tensile testing as given in Fig. 17(b). This propensity for the formation of deformation bands at 54° to the direction of first principal stress has been noted previously in the literature [31,32]. Considering then the material deforming between each roller contact point, 17.5 mm between centres, and a specimen width of 20 mm the highest localised neck angle that can form is 48°, much lower than the 54° normally observed, as schematically shown in Fig. 17(c). This could be the one of the main reasons for the delay in localised necking in the case of repetitive bending under tension samples as the material in the gauge section remains in the state of diffused necking throughout the test (indicated by the blue dotted rectangle in Fig. 17(a)). The dotted line in blue shows the two extremes of the bending assembly travel. A further factor influencing the enhanced uniform elongation in the repetitive bending under tension is that the displacement of the deformation zone occurring along the gauge section due to the movement of the roller bending assembly leads to the suppression of localised necking at one particular location.

Stress triaxialities of the material subjected to R-BUT along the 0RD and 45RD were presented in Figs. 12 and 13. It was shown that with increasing penetration, stress triaxiality becomes more negative. In previous studies, it was shown that damage in the negative triaxiality (from −0.33 to 0) regions is decreased due to the suppression of shear damage and decrease in shear deformation [33,34]. It has also been reported that accelerated damage (decrease in fracture strain) was observed between triaxialities of −0.667 and −0.33 due to shear deformation. It was found that there is always a competition between the two major damage mechanisms in negative triaxiality regions (less than −1/3). The first mechanism is void volume increase due to the hydrostatic

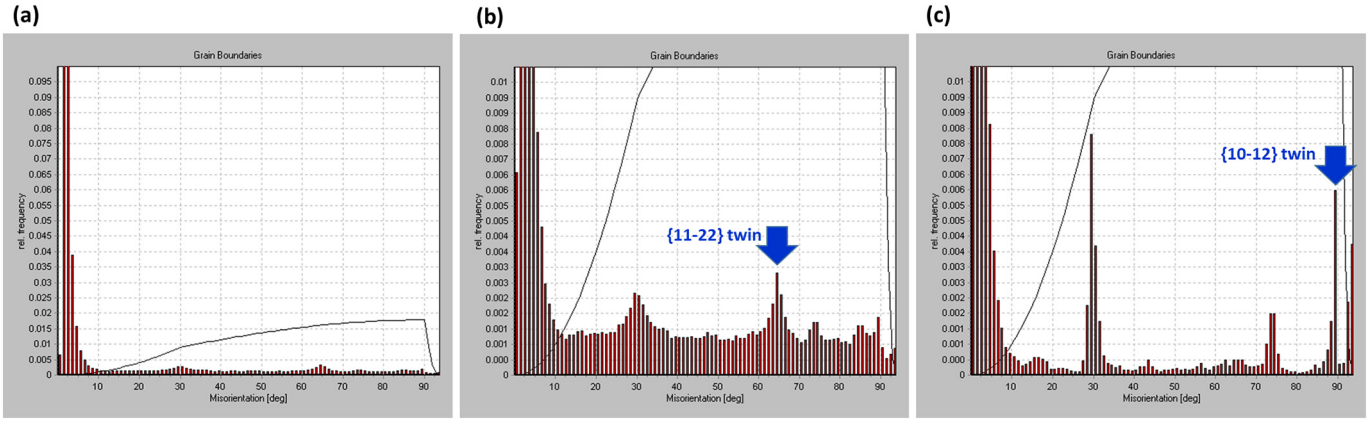

Fig. 18. Grain boundary misorientation histograms based on EBSD scans done on Ti50A alloy samples: (a) as-received, (b) after tensile testing and (c) after repetitive bending under tension testing.

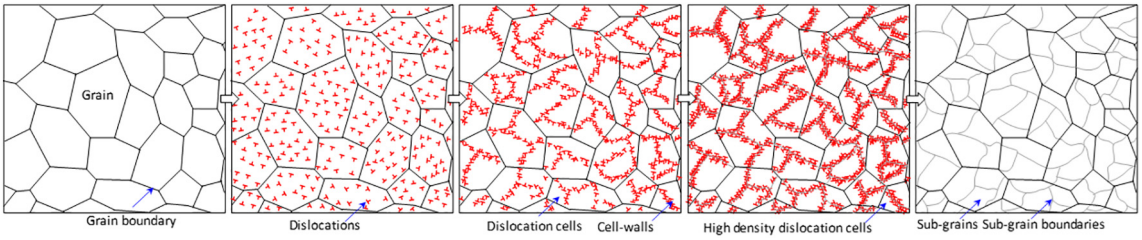

Fig. 19. Schematic representation of microstructural changes occurring with the pre-existing grains during bending and unbending.

stress arising from the shear deformation component while the second is the decrease of void volume due to a negative hydrostatic stress in this triaxiality regime. In the present study, it was observed during the experiments that fracture strain increases for the 0.88 mm and 1.25 mm penetrations, while it decreased for 4 mm penetration as shown in Fig. 3. This may be understood in terms of the above explanations which suggest that as negative triaxiality goes below −0.33 the damage mechanism shifts from one mode to the other. This statement seems to be true for the present study (as shown in Figs. 12 and 13) that up to a penetration value of 1.25 mm the negative triaxiality values are in the range of −0.4 to −0.33. While for a penetration = 4 mm, the negative triaxiality value goes below −0.4 and hence the decrease in fracture strain due to switch between the two competing damage mechanisms as explained before.

It is noticeable that the required tensile force in the repetitive bending is less than that required for plastic deformation in the conventional tensile testing as shown in Fig. 3. Similar results are also found through FE simulations though are not presented here for brevity. In the R-BUT testing, the sheet is subjected to several cycles of bending as it passes through the roller assembly. As per standard bending theory, this means that part of the sheet will be in tension and part in compression – the associated areas reversing as the sheet progresses through all three rollers. Hadoush et al. [15] suggested that the tensile force required for deforming the strip depends on how much of the cross section is under compression. Depending on the testing parameters, the neutral line can move towards the surfaces. Therefore, the overall tensile force in R-BUT is less than that measured in the standard tensile test. As a consequence, the sections of the sample above and below the bending zone are under lesser loads which may not be sufficient to cause any plastic deformation. In other words, while the sample is undergoing bending and unbending, the rest of the sample remains in the elastic regime only. By progressing the repetitive bending under tension test, the thickness as well as the width (i.e. the cross-section area) of the sample continuously decreases along the entire length as shown in

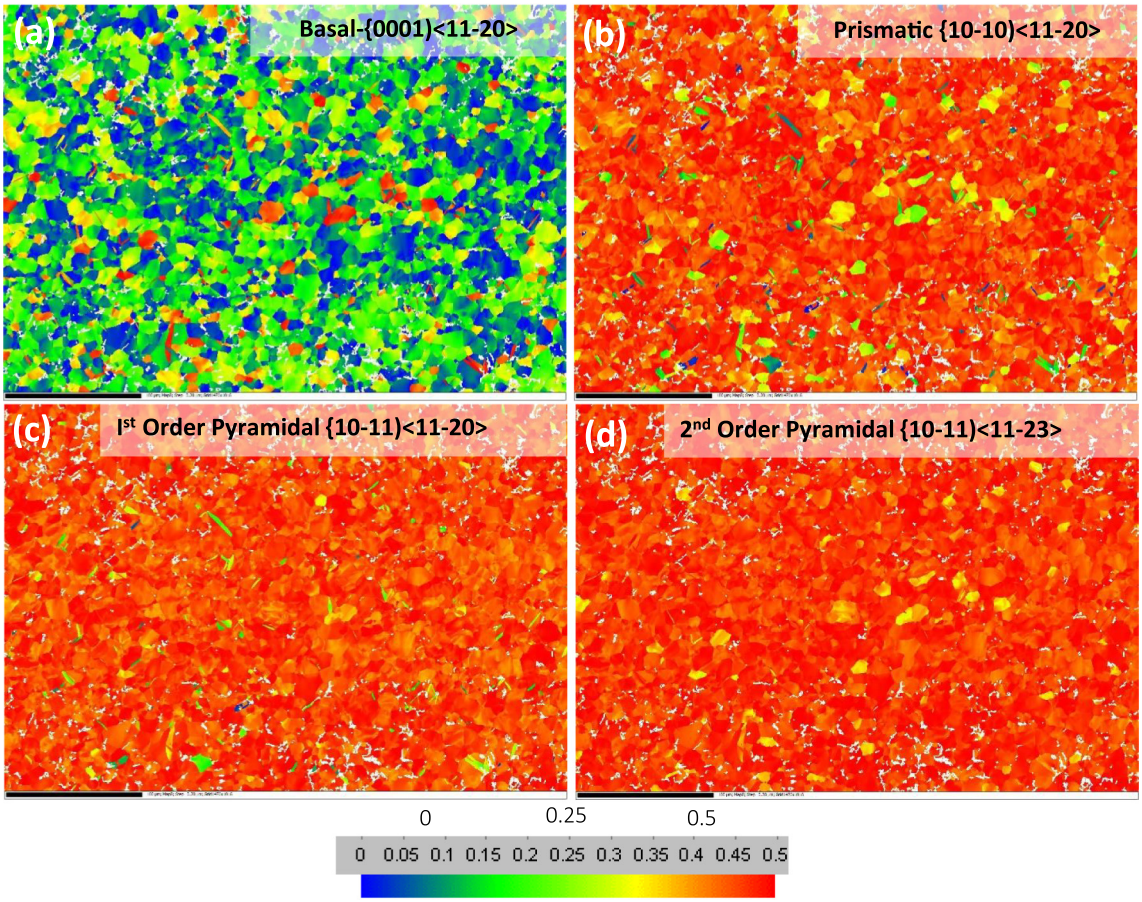

Fig. 20. Schmid factor maps of possible slip systems expected to activate in the case of Ti50A sample subjected to tensile testing: (a) {0001}<11-20> basal, (b) {10-10}<11-20> prismatic, (c) {10-11}<11-20> first order pyramidal and (d) {10-11}<11-23> second order pyramidal.

Fig. 4(b). This may raise the longitudinal stress applied on the sample until the yield stress is exceeded. If this occurs, the plastic deformation would become delocalised and progress globally.

The mechanism for the final fracture of the sample subjected to the repetitive bending under tension is not clear yet. The roller movement along the gauge section may lead to deterioration of the surface roughness of the gauge sections in the tested samples which may trigger initiation of micro cracks leading to failure of the samples. This may be an effective limit for the repetitive bending under tension tests at the higher traverse speeds shown in Fig. 5.

Another influencing factor could be microstructural changes occurring dynamically in the matrix of the sample falling into the gauge section. Microstructural analysis of samples after tensile testing and repetitive bending under tension has confirmed the activation of deformation twins within the deforming grains. Formation of these twins within the grains is a result of the local strain incompatibility produced by dislocation slip in grain boundary areas. Grains with a high Schmid factor are expected to activate these deformation twins. The orientations $\{10\bar{1}2\}$, $\{1\bar{1}21\}$ and $\{1\bar{1}22\}$ are three commonly observed deformation twinning modes in titanium at room temperature. A grain boundary misorientation histogram from the EBSD results of the as-received condition given in Fig. 18(a) confirmed the presence of grains of α phase without any deformation twins. Fig. 18(b) shows the misorientation histogram from the sample that went up to fracture during tensile testing showing a major peak around 65° with a rotation axis of $<10\bar{1}0>$, corresponding to $\{1\bar{1}22\}$ twin boundaries. The histogram shows a noticeable peak of misorientation at around 90°, which would indicate that these boundaries correspond to the $\{10\bar{1}2\}$ tensile twin boundary (Fig. 18(c)). Formation of twins is always accompanied by a certain accommodative deformation in their immediate neighbourhoods, depending on the deformation modes available. Evidence for formation of fine grains is shown by the EBSD scans on the RD-TD and RD-ND planes. Dislocations generated during the bending process are expected to undergo polygonisation as a result of recovery during the unbending stage. TEM investigations suggested that the presence of stress concentrations in the form dislocation pile-ups within the α phase is the main mechanism behind the occurrence of recovery in Titanium alloys at room temperature [35]. So in the present case also a similar mechanism may play a role in recovery occurring in the sample subjected to R-BUT.

Additionally, the deformation mechanism of repetitive bending under tension is similar to that occurring in samples subjected to a process called repetitive corrugation and straightening (RCS) [36,37]. This process is also called constrained groove pressing by Shin et al. [38], or repeated shear deformation by Huh et al. [39]. RCS is a top-down

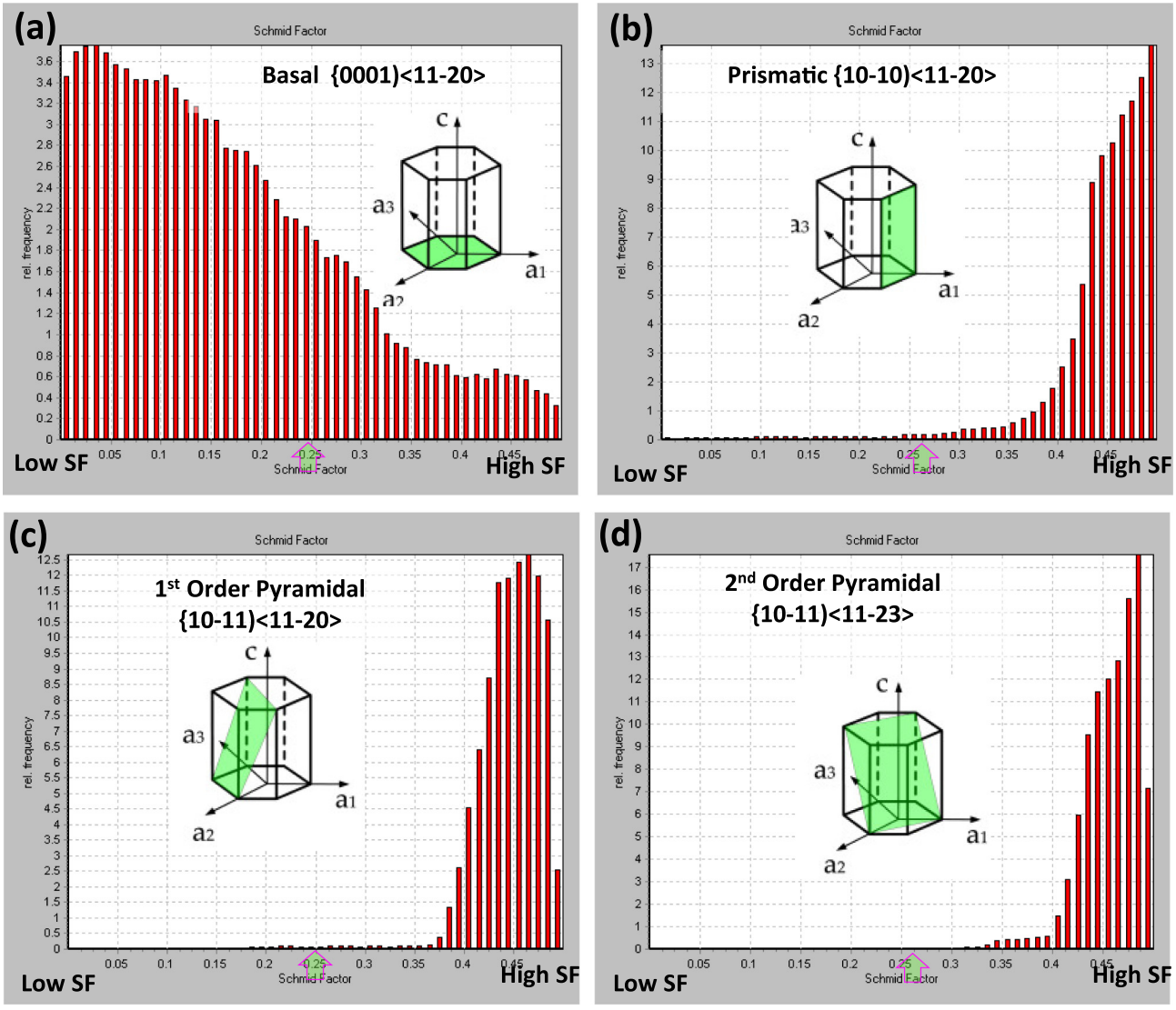

Fig. 21. Histograms of possible slip systems in the case of Ti50A sample subjected to tensile testing: (a) {0001}<11-20> basal, (b) {10-10}<11-20> prismatic, (c) {10-11}<11-20> first order pyramidal and (d) {10-11}<11-23> second order pyramidal slip systems.

approach adopted by researchers to obtain ultra-fine grains in the processed materials. The mechanism of grain refinement in the case of RCS includes increasing dislocation density within the grains followed by formation of dense dislocations walls and then converting dislocation walls into high-angle grain boundaries. In the RCS process the sheet material is repetitively bent and straightened under plane strain deformation condition without a noticeable change in the cross-section. The principle behind this process is that the material undergoes repetitive shear deformation by alternate pressing with the help of an asymmetrically grooved die and a flat die. The large plastic strains which are imposed during the RCS process lead to grain refinement. In the R-BUT process however, due to the higher number of cycles than used for the RCS process, the samples experience a higher level of shear plastic strain. The EBSD results given in Figs. 9 and 10 show the formation of sub-grains within the deformation bands in the sample subjected to repetitive bending under tension. This is due to the high levels of shear plastic deformation induced by bending and unbending. Through the process, grains are initially divided into cell boundaries containing dislocation cells, this is followed by formation of sub-grains from cell boundaries as well as dislocation cells. As the amount of shear strain imposed on the material increases, the misorientation across sub-grain boundaries increases and eventually becomes large enough to transform the sub-grain boundaries which are low-angle grain boundaries to high-angle grain boundaries. The schematic given in Fig. 19 explains a possible mechanism of grain fragmentation as result of strain assisted dislocation activation in the material.

This grain refinement process may function as an accommodation process for the intense plastic strain generated by the bending deformation with the internal energy generated by the high dislocation density acting as the driving force. The formation of fine grains as a result of recovery within the pre-existing grains functions to reduce the dislocation density which in turn leads to a reduction in the strain hardening behaviour of the test samples. This is clearly evidenced from the load-displacement curves shown in Figs. 3 and 5. In the case of a normal tensile test, as the amount of strain imposed increases the number of slip systems activated within each grain increases. Also the number of dislocation sources activated increases with strain which leads to an increase in dislocation density. As a result of slip activities, the interaction of dislocations (dislocation pile-up) with the grain boundaries occurs and leads to formation of voids. These voids grow under the influence of the tensile force applied and finally lead to fracture. Fracture studies carried out on the samples that underwent normal tensile testing and repetitive bending under tension confirmed that a higher fraction of voids was formed in the samples after tensile testing as shown in Figs. 15 and 16.

Figs. 20 and 21 show the Schmid factor maps and histograms of the main slip systems expected to activate in the matrix having only grains of α phase of the Ti50A sample subjected to tensile testing: (a) {0001} <11-20> basal, (b) {10-10} <11-20> prismatic, (c) {10-11} <11-20> first order pyramidal and {10-11} <11-23> first order pyramidal slip systems. The Schmid factor frequency distribution in the histograms of prismatic and pyramidal slip systems confirmed that prismatic and pyramidal slip systems were activated in the majority of grains during tensile loading (Fig. 20). Note that plastic deformation is expected to occur preferentially in the grains having a higher Schmid factor value.

Figs. 22 and 23 shows the Schmid factor maps and histograms of the main slip systems expected to activate in the sample subjected to

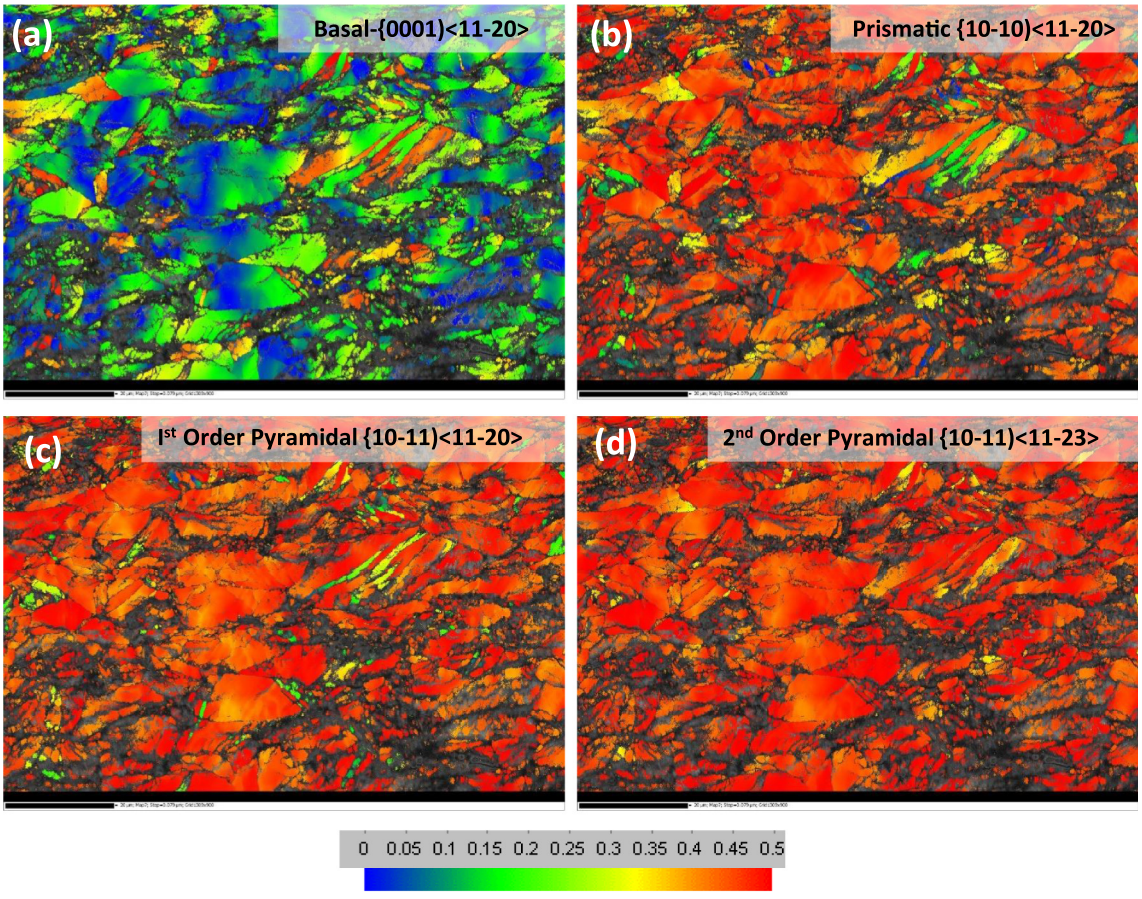

Fig. 22. Schmid factor maps of possible slip systems expected to activate in the case of Ti50A sample subjected to repetitive bending under tension testing: (a) {0001} <11-20> basal, (b) {10-10} <11-20> prismatic, (c) {10-11} <11-20> first order pyramidal and (d) {10-11} <11-23> second order pyramidal systems.

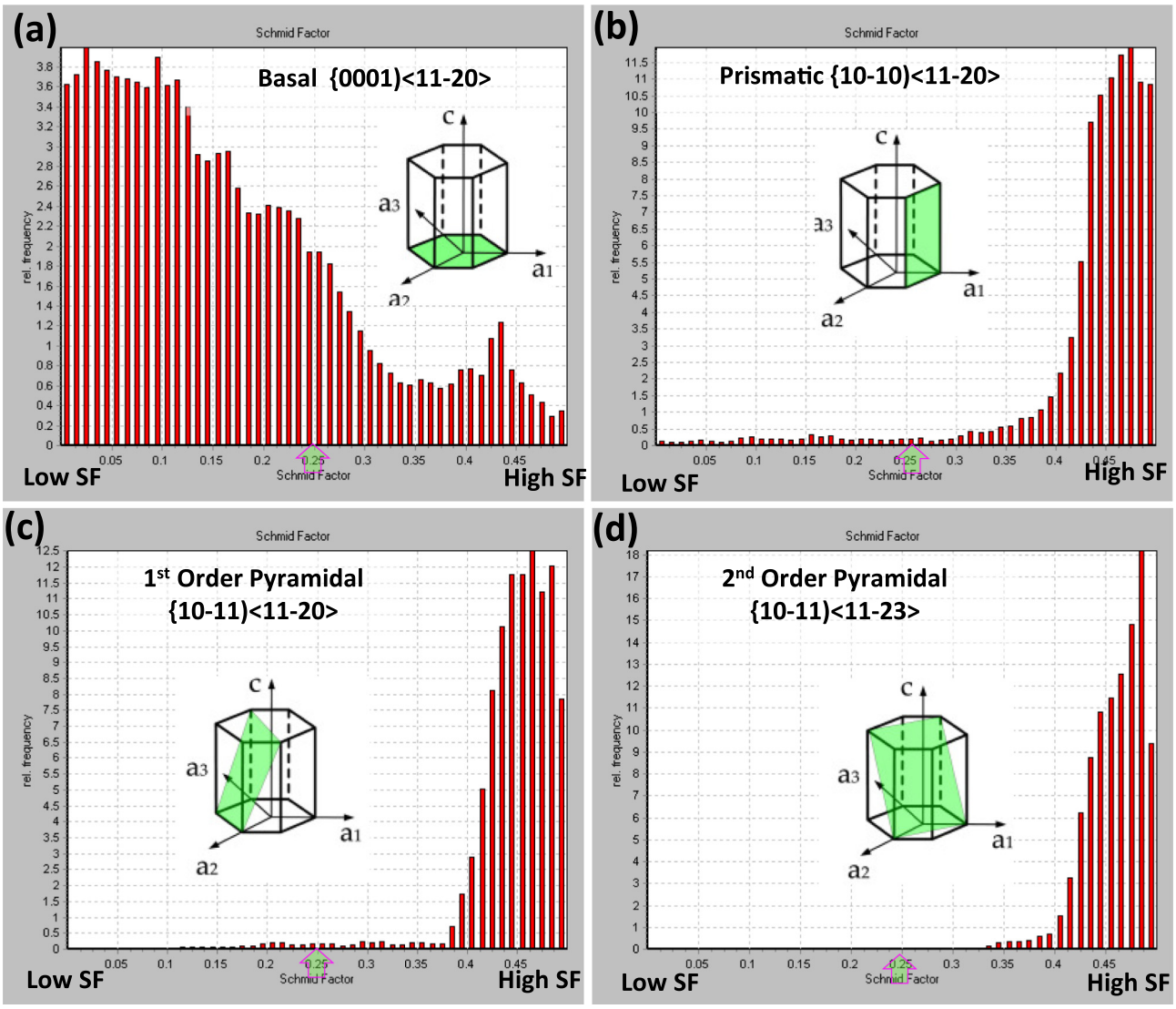

Fig. 23. Histograms of possible slip systems in the case of Ti50A sample subjected to repetitive bending under tension testing: (a) {0001} <11-20> basal, (b) {10-10} <11-20> prismatic, (c) {10-11} <11-20> first order pyramidal and (d) {10-11} <11-23> first order pyramidal slip systems.

repetitive bending under tension testing at room temperature: (a) {0001} <11-20> basal, (b) {10-10} <11-20> prismatic, (c) {10-11} <11-20> first order pyramidal and (d) {10-11} <11-23> second order pyramidal slip systems. The Schmid factor frequency distribution from the histograms shown in Fig. 23 consists of Schmid factor values higher than 0.25 for the prismatic systems and values higher than 0.35 in the case of pyramidal slip systems. This confirmed that prismatic and pyramidal slip systems are getting activated in the majority of grains during repetitive bending under tension testing.

5. Conclusions

This work aimed to study the deformation behaviour of Ti50A alloy through repetitive bending under tension conditions and comparing this with conventional tensile testing. In this work, a bespoke testing rig was designed, manufactured and used to study the properties of Ti-50A alloy under R-BUT loading condition. During repetitive bending under tension test conditions, the bending zone (i.e. plastic deformation zone) moves along the gauge section of the sample. The main findings can be summarized as follows:

- Moving the plastic deformation zone leading to a delay in localised necking occurring during R-BUT testing made it possible to deform samples of Ti-50A alloy to very high strains under lower required forces as compared to the standard tensile testing. In addition to that, the total elongation of the samples subjected to R-BUT was significantly enhanced as compared to samples subjected to conventional tensile testing.
- R-BUT test results indicate that the force required to stretch the sample, and also the uniform elongation obtained, are strongly dependent on the testing parameters e.g. bending package velocity and bending level. It has been illustrated that in some configurations of repetitive bending under tension, enhanced plasticity can be achieved at room temperature.
- Finite element analysis confirmed that the enhancement in the elongation in the samples subjected to R-BUT could be due to a non-uniform distribution of stress triaxiality along the gauge section and also due to the contact areas under the rollers exhibiting negative stress triaxialities.
- EBSD analysis carried out on samples after R-BUT confirmed the formation of sub-grains which could be a due re-arrangements of dislocations as a result of recovery processes occurring

dynamically during bending and un-bending of the sample under tension.

Crystal plasticity finite element method (*CPFEM*) based simulations will be employed for further understanding of microstructural evolution, deformation behaviour and failure of the alloy subjected to R-BUT, which will be reported in future.

Supplementary data to this article can be found online at https://doi.org/10.1016/j.matdes.2020.108814.

CRediT authorship contribution statement

Saeed Tamimi: Conceptualization, Methodology, Investigation, Writing - original draft, Writing - review & editing. **Giribaskar Sivaswamy:** Investigation, Writing - original draft, Writing - review & editing. **M. Amir Siddiq:** Formal analysis, Writing - original draft, Writing - review & editing. **Alan Leacock:** Conceptualization, Writing - review & editing. **Paul Blackwell:** Validation, Writing - review & editing.

Declaration of competing interest

The authors declare that they have no known competing financial interests or personal relationships that could have appeared to influence the work reported in this paper.

Acknowledgment

The authors wish to acknowledge financial and technical support for this work from the Advanced Forming Research Centre's Tier 1 members through the Core research programme.

References

[1] P. Eyckens, et al., Small-scale finite element modelling of the plastic deformation zone in the incremental forming process, Int. J. Mater. Form. 1 (1) (2008) 1159–1162.
[2] S. He, et al., Finite element modeling of incremental forming of aluminum sheets, Advanced Materials Research, Trans Tech Publ, 2005.
[3] C. Henrard, et al., Comparison of FEM simulations for the incremental forming process, Advanced Materials Research, Trans Tech Publ, 2005.
[4] Z. Liuru, Study of Fender NC Incremental Sheet Metal Forming, 2009.
[5] F.C. Minutolo, et al., Forces analysis in sheet incremental forming and comparison of experimental and simulation results, Intelligent Production Machines and Systems, Elsevier 2006, pp. 229–234.
[6] N.V. Reddy, J. Cao, Incremental Sheet Metal Forming: A Review, Department of Mechanical Engineering, Indian Institute of Technology Kanpur, Kanpur, India, 2009 nvr@ iitk. ac. in.
[7] P. Martins, et al., Theory of single point incremental forming, CIRP Ann. 57 (1) (2008) 247–252.
[8] F.C. Minutolo, et al., Evaluation of the maximum slope angle of simple geometries carried out by incremental forming process, J. Mater. Process. Technol. 194 (1–3) (2007) 145–150.
[9] M. Yamashita, M. Gotoh, S.-Y. Atsumi, Numerical simulation of incremental forming of sheet metal, J. Mater. Process. Technol. 199 (1–3) (2008) 163–172.
[10] N. Devarajan, et al., Complex incremental sheet forming using back die support on aluminium 2024, 5083 and 7075 alloys, Procedia Engineering 81 (2014) 2298–2304.
[11] I. Eipert, et al., Improvement in ductility in commercially pure titanium alloys by stress relaxation at room temperature, Key Engineering Materials, Trans Tech Publ, 2014.
[12] J. Benedyk, N. Parikh, D. Stawarz, A method for increasing elongation values for ferrous and nonferrous sheet metals(ferrous and nonferrous sheet metals neck formation prevention for increasing elongation in tensile tests, using continuous plastic bending method), J. Mater. 6 (1971) 16–29.
[13] J. Hu, Z. Marciniak, J. Duncan, Mechanics of Sheet Metal Forming, Elsevier, 2002.
[14] W. Emmens, A.H. van den Boogaard, An overview of stabilizing deformation mechanisms in incremental sheet forming, J. Mater. Process. Technol. 209 (8) (2009) 3688–3695.
[15] A. Hadoush, A.H. van den Boogaard, W. Emmens, A numerical investigation of the continuous bending under tension test, J. Mater. Process. Technol. 211 (12) (2011) 1948–1956.
[16] H. Iseki, K. Kato, S. Sakamoto, Forming limit of flexible and incremental sheet metal bulging with a spherical roller, Advanced Technical Plastics 1 (1) (1993) 1635–1640.
[17] R. Schleich, et al., Investigation on the effect of curvature and sheet thickness on forming limit prediction for aluminium sheet metal alloys, Int. J. Mater. Form. 2 (1) (2009) 411.
[18] J. Allwood, D. Shouler, A.E. Tekkaya, The increased forming limits of incremental sheet forming processes, Key Engineering Materials, Trans Tech Publ, 2007.
[19] J.M. Allwood, D.R. Shouler, Generalised forming limit diagrams showing increased forming limits with non-planar stress states, Int. J. Plast. 25 (7) (2009) 1207–1230.
[20] P. Eyckens, A. Van Bael, P. Van Houtte, Marciniak–Kuczynski type modelling of the effect of through-thickness shear on the forming limits of sheet metal, Int. J. Plast. 25 (12) (2009) 2249–2268.
[21] T. Sawada, G. Fukuhara, M. Sakamoto, Deformation mechanism of sheet metal in stretch forming with computer numerical control machine tools, Journal-Japan Society for Technology of Plasticity 42 (10; ISSU 489) (2001) 1067–1069.
[22] W. Emmens, A.H. van den Boogaard, Incremental forming by continuous bending under tension—an experimental investigation, J. Mater. Process. Technol. 209 (14) (2009) 5456–5463.
[23] S. Tamimi, et al., Asymmetric rolling of interstitial free steel sheets: microstructural evolution and mechanical properties, J. Manuf. Process. 31 (2018) 583–592.
[24] M. Zecevic, et al., Residual ductility and microstructural evolution in continuous-bending-under-tension of AA-6022-T4, Materials 9 (3) (2016) 130.
[25] Q. Yang, et al., Effect of multi-pass bending deformation on microstructure evolution and mechanical properties of AZ31 alloy sheet, Mater. Res. 19 (2) (2016) 322–327.
[26] I. ASTM, ASTM E8/E8M-16a: Standard Test Methods for Tension Testing of Metallic Materials, ASTM International, West Conshohocken, PA, USA, 2016.
[27] D. Palousek, et al., Effect of matte coating on 3D optical measurement accuracy, Opt. Mater. 40 (2015) 1–9.
[28] H.S. Turkmen, et al., On the mechanical behaviour of AA 7075-T6 during cyclic loading, Int. J. Fatigue 25 (4) (2003) 267–281.
[29] F. Bridier, et al., Crystal plasticity modeling of slip activity in Ti–6Al–4V under high cycle fatigue loading, Int. J. Plast. 25 (6) (2009) 1066–1082.
[30] A. Siddiq, et al., Springback in Single Point Incremental Sheet Metal Forming. ESAFORM 2013, 2013.
[31] S.F. Keeler, W.A. Backofen, Trans. Am. Soc. Met. 56 (1963) 25–48.
[32] W.A. Backofen, Deformation Processing, Addison-Wesley Publishing Company, 1972.
[33] S. Kweon, Damage at negative triaxiality, European Journal of Mechanics-A/Solids 31 (1) (2012) 203–212.
[34] Y. Bao, T. Wierzbicki, On fracture locus in the equivalent strain and stress triaxiality space, Int. J. Mech. Sci. 46 (1) (2004) 81–98.
[35] M. Savage, T. Neeraj, M. Mills, Observations of room-temperature creep recovery in titanium alloys, Metall. Mater. Trans. A 33 (3) (2002) 891–898.
[36] J. Huang, et al., Microstructures and dislocation configurations in nanostructured Cu processed by repetitive corrugation and straightening, Acta Mater. 49 (9) (2001) 1497–1505.
[37] N. Thangapandian, S.B. Prabu, K. Padmanabhan, Effects of die profile on grain refinement in Al–Mg alloy processed by repetitive corrugation and straightening, Mater. Sci. Eng. A 649 (2016) 229–238.
[38] D.H. Shin, et al., Constrained groove pressing and its application to grain refinement of aluminum, Mater. Sci. Eng. A 328 (1–2) (2002) 98–103.
[39] M.Y. Huh, H. Kim, O. Engler, Evolution of texture and microstructure during repeated shear deformation in aluminum 1100 alloy sheets, Materials Science Forum, Trans Tech Publications, 2002.